A consistent dimensional analysis of gas–liquid mass transfer in an aerated stirred tank containing purely viscous fluids with shear-thinning properties

Raouf Hassan[a,b], Karine Loubiere[c,d,*], Jack Legrand[a,b], Guillaume Delaplace[e]

[a] Université de Nantes, Laboratoire GEPEA, CRTT, 37 boulevard de l'université, BP 406, F-44602 Saint-Nazaire, France
[b] CNRS, Laboratoire GEPEA, F-44602 Saint-Nazaire, France
[c] Université de Toulouse, INPT, UPS, Laboratoire de Génie Chimique (LGC), 4 allée Emile Monso, BP 84234, F-31432 Toulouse, France
[d] CNRS, Laboratoire de Génie Chimique (LGC), F-31432 Toulouse, France
[e] INRA, Laboratoire PIHM UR 638, 369 Rue Jules Guesde, BP 39, F-59651 Villeneuve d'Ascq Cedex, France

* Corresponding author. Tel.: +33 0 5 34 32 36 19; fax: +33 0 5 34 32 36 97.
E-mail address: Karine.Loubiere@ensiacet.fr (K. Loubiere).

A B S T R A C T

This paper deals with gas–liquid mass transfer in an aerated stirred tank containing Newtonian or shear-thinning fluids. The aim is to demonstrate that, for a given mixing system, an unique dimensionless correlation gathering all the mass transfer rates (150 k_la measurements) can be obtained if and only if the variability of the rheological material parameters is correctly considered when implementing the theory of similarity. More particularly, it is clearly illustrated that a too gross simplification in the relevant list of the parameters characterizing the dependence of apparent viscosity with shear rates leads to pitfalls when building the π-space set. This is then a striking example showing that a robust predictive correlation can be established when the non-constancy of fluid physical properties ceases to be neglected.

Keywords:
Dimensional analysis
Variable material property
Gas–liquid mass transfer
Shear-thinning fluids
Aerated stirred tank
Model of Williamson–Cross

1. Introduction

The dispersion of a gaseous phase in a liquid phase for mass transfer purposes is involved in many processes, in the field of chemical reaction engineering (e.g. for chlorinations, hydrogenations, oxidations, alkylations, ammonolysis and so forth) but also in biochemical engineering (including fermentation, waste water treatment). The use of agitated tanks is a widespread practice for operating such absorption processes as offering the advantages to generate high interfacial areas and intense mixing of liquid phase. Understanding and modelling mass transfer between phases is of importance, because it may often become the critical step determining the achievement of the application, and thus may give the main guidelines on which the design and the scale-up of the process will be based. The transferred mass quantity depends on the solute solubility in the liquid phase, but above all on the interfacial area, a, and on the overall liquid-phase mass transfer coefficient, K_l. The product of these latter parameters is commonly called absorption rate coefficient or overall volumetric gas–liquid mass transfer coefficient (K_la or k_la for low soluble gases). The factors influencing of such unit operation (in particular K_la) are very large, including tank geometry and dimensions, impeller type, dimensions and rotational impeller speed, aeration system and gas flow rate, physical and rheological properties of gas and liquid phases, temperature, and pressure. In an attempt to elucidate the effects of the latter parameters on the absorption rate coefficient, a great amount of published investigations are encountered in the literature; some interesting overviews are given in [1–5]. They provide improved knowledge on gas–liquid mass transfer through experimental data, empirical correlations, mechanistic analysis or more recently numerical simulations.

Most of them deal with the cases when the liquid phase is a *Newtonian fluid* with low viscosities. From various sets of experiments carried out at lab-scale and/or at larger scale, some empirical correlations for k_la are proposed, involving either dimensional or dimensionless parameters. At present, the most frequently used dimensional correlation remains the one of Van't Riet [6] or some variants in which the constant and exponents have been modified. They are expressed such as:

$$k_la = C \cdot (U_g)^{C_1} \cdot \left(\frac{P}{V_l}\right)^{C_2} \cdot (\mu)^{C_3} \quad (1)$$

where the constant C is strongly affected by the geometrical parameters of the agitation system, and μ is the Newtonian viscosity. Garcia-Ochoa and Gomez [3] recently summarized the different exponents associated with Eq. (1) that are available in the literature.

Nomenclature

a	specific interfacial area (m^{-1})
C_{O_2}	concentration in dissolved oxygen (kg/m^3)
$C^*_{O_2}$	concentration in dissolved oxygen at saturation (kg/m^3)
d	air sparger diameter (m)
D	impeller diameter (m)
$\mathcal{D}$	oxygen diffusion coefficient in the liquid phase (m^2/s)
G/V_l	mass throughout per unit of liquid volume ($kg/s/m^3$)
g	gravity acceleration (m/s^2)
H	Henry's constant (Pa)
H_t	tank height (m)
k_l	liquid-side mass transfer coefficient (m/s)
K	consistency index from the model of Ostwald–de-Waele (Eq. (14)) ($Pa\,s^{n_{ost}}$)
K_l	overall mass transfer coefficient (m/s)
k_la	overall volumetric gas–liquid mass transfer coefficient (s^{-1})
K_{MO}	Metzner–Otto constant (Eq. (5))
m	Henry's constant
n_{ost}	flow index from the model of Ostwald–de-Waele (Eq. (14))
n_w	flow index from the model of Williamson–Cross (Eq. (15))
N	rotational impeller speed (s^{-1})
P/V_l	power dissipated per unit of volume (W/m^3)
P_s	pressure in the system (Pa)
Q_g	gas flow rate (m^3/s)
t	time (s)
t_w	time parameter from the model of Williamson–Cross (Eq. (15)) (s)
T_l	temperature of the liquid phase (K)
T_t	vessel diameter (m)
U_g	superficial gas velocity (m/s)
V	tank volume (m^3)
V_l	liquid tank volume (m^3)

Greek letters

ε	mean standard deviation (Eq. (50))
$\dot{\gamma}$	shear rate (s^{-1})
$\dot{\gamma}_o$	reference shear rate (s^{-1})
$\dot{\gamma}_{av}$	average shear rate defined from the Metzner–Otto concept (Eq. (4)) (s^{-1})
μ	dynamic viscosity (Pa s)
μ_a	apparent viscosity (Pa s)
μ_o	reference apparent viscosity parameter defined at reference shear rate (Pa s)
μ_w	viscosity parameter from the model of Williamson–Cross (Eq. (15)) (Pa s)
υ	cinematic viscosity (Pa s)
ρ	density (kg/m^3)
σ	surface tension (N/m)

Dimensionless numbers

Fr	Froude number (Eq. (27))
k_la^*	dimensionless volumetric mass transfer coefficient (Eq. (25))
μ^*	dimensionless viscosity (Eq. (29))
π_i	dimensionless number deduced from the theory of similarity
ρ^*	dimensionless density (Eq. (28))
σ^*	dimensionless surface tension (Eq. (30))
Sc	Schmidt number defined according to gas phase properties (Eq. (31))
t^*_w	dimensionless time number issued from the Williamson–Cross's model (Eq. (45))
U^*_g	dimensionless superficial gas velocity (Eq. (26))

Subscripts

g	gas phase
l	liquid phase

Another approach is to use correlations with *dimensionless groups*; contrary to dimensional correlations, they guarantee firm basis for process scale-up, provided that they must be established with respect to the theoretical context of the theory of similarity. The pioneer work's of Zlokarnik [7] has established the relevant list of influencing intensive parameters and proposed the following dependence between dimensionless numbers:

$$(k_la)^* = f_1\left\{\left(\frac{P}{Q_g}\right)^*, \left(\frac{Q_g}{V_l}\right)^*, \sigma^*, Sc, Si^*\right\}$$

$$\text{where}\quad \begin{cases} (k_la)^* = k_la\cdot\left(\dfrac{\upsilon_l}{g^2}\right)^{1/3}, & \left(\dfrac{P}{Q_g}\right)^* = \left(\dfrac{P}{Q_g}\right)\cdot[\rho_l\cdot(\upsilon_l\cdot g)^{2/3}]^{-1}, \\ \sigma^* = \sigma\cdot[\rho_l\cdot(\upsilon_l^4\cdot g)^{1/3}]^{-1}, & \left(\dfrac{Q_g}{V_l}\right)^* = \left(\dfrac{Q_g}{Vl}\right)\cdot\left(\dfrac{\upsilon_l}{g^2}\right)^{1/3} \end{cases} \quad (2)$$

Note that, in Eq. (2), Sc is the Schmidt number and Si^* is a material dimensionless parameter which describes coalescence behaviour of solutions (i.e. ionic strength, electrical charge of ions, . . .). Thanks to this approach, Zlokarnik [7] could rigorously distinguish different process relationships depending whether the system is coalescent or non-coalescent.

Few years later, Judat [8] has critically examined the existing publications on gas–liquid mass transfer (coalescing systems) in stirred vessels. Description of experimental data with the aid of intensive parameters has leaded this author to (±30% deviation):

$$(k_la)^* = 9.8\times10^{-5}\cdot\frac{(P/V_l)^{*0.40}}{B^{-0.6}+0.81\times10^{-0.65/B}} \quad (3)$$

where $B = (Q_g/T_t^2)\cdot(\upsilon_l\cdot g)^{-1/3}$, the others numbers being defined as in [7]. Judat [8] has then shown that a monoparametric representation of $(k_la)^*$ versus $(P/V_l)^*$ is inadequate, and that only a π-space representation containing both dimensionless power per unit volume and superficial gas velocity can satisfactorily correlate $(k_la)^*$. This author has also put forward that another π-space, containing non intensive parameters (rotational impeller speed instead of power per unit liquid volume) could be used to describe the measures of $(k_la)^*$, but this π_i-space is larger than the previous one.

Few authors (for example [9,10]) have conserved the dimensionless group $(k_la)^* = k_la\cdot(\upsilon_l/g^2)^{1/3}$ defined by these two pioneer works for modelling absorption processes. Most of them have adopted, with or without theoretical backgrounds, others definitions for making dimensionless k_la [11–17]. They include notably a modified Sherwood number $(k_la\cdot T_t^2/\mathcal{D})$ or Stanton number $(k_la\cdot V_l/Q_g)$ [3].

When *shear-thinning fluids* are involved, two additional questions arise unfortunately in a point of view of the theory of similarity:

- How should we proceed to guarantee that the results obtained with Newtonian fluids can be extended to these non-Newtonian liquids? The spatial distribution of liquid viscosity in the tank, due to its dependency with shear rates, constitutes a major difficulty with regard to the choice of a representative viscosity.

Table 1
Dimensions of the experimental setup.

Tank size	$T_t = 0.212$ m
	$H_t = 0.316$ m
	$V = 10$ L
	$H_l = 0.212$ m
	$V_l = 7.4$ L
Baffles	$w_b = T_t/10$ (width, in m)
	$b_b = T_t/50$ (distance from walls, in m)
Impeller (six-concave-blade turbine)	$D = 0.4{\cdot}T_t$ (impeller diameter, in m)
	$D_s = 3{\cdot}T_t/4$ (disk diameter, in m)
	$C = T_t/4$ (clearance from the bottom, in m)
	$b = D/5$ (blade height, in m)
	$w = 0.5\ D/5$ (blade width, in m)
	$l = D/4$ (blade length, in m)
Sparger	$d = D$ (sparger diameter, in m)

- How should we proceed to guarantee that the results obtained at lab-scale will be also scalable at industrial scale?

Until now, most of works encountered in the literature did not take care about these questions: they simply consist in replacing the Newtonian viscosity by an apparent viscosity defined from the Ostwald–de-Waele's model in which an average shear rate is considered according to the well-known concept of Metzner–Otto:

$$\dot{\gamma}_{av} = K_{MO} \cdot N \tag{4}$$

where the constant K_{MO} depends on the agitation system. Such choice of apparent viscosity is in many cases questionable, in particular when (i) the flow regime is not laminar (the use of Eq. (4) becomes then quite haphazard) and (ii) the rheological behaviour of fluids cannot be described in the whole range of shear rates by the Ostwald–de-Waele's model.

The present paper aims at rigorously answering these two latter questions, starting from the theoretical background underlying the dimensional analysis and extending it to the cases of variable material properties. More accurately, the objective is to show how to proceed: (i) to construct a complete list of relevant parameters able to consider variable rheological parameters, and consequently (ii) to elaborate, without pitfalls, a set of dimensionless numbers characterizing all the factors governing absorption rate coefficients ($k_l a$) in an aerated stirred tank where purely viscous fluids with or without shear-thinning properties are involved. To support this theoretical approach, a set of experiments was carried out to measure $k_l a$ in a stirred tank aerated in volume. Different operating conditions (rotational impeller speed, gas flow rate) were covered as well as various fluids (seven purely viscous fluids of which four have shear-thinning properties).

2. Materials and methods

2.1. Experimental set-up

As shown in Fig. 1, the experimental set-up consisted of a cylindrical PMMA vessel of 10 L with a curved bottom. It was equipped with a square double jacket (27.2 cm × 27.2 cm) and four baffles in stainless steel mounted perpendicular to the vessel wall. Table 1 presents the geometrical details of the tank. The agitation system was composed of a home-made six-concave-blades disk turbine which dimensions were respectful for the ones implemented in commercial CD6 Chemineer® impellers. The rotational impeller speed (N) was regulated by using an electrical motor (Ikavisc MR-D1 Messrührer, Janke & Kunkel, Ika®), and varied from 200 to 1000 rpm.

Gas (air or nitrogen) was fed into the tank using a ring sparger with a diameter equal to the impeller diameter, as recommended by [18]. The latter was composed by 20 holes of 0.5 mm in diameter. The sparger was located 30 mm from the bottom of the tank, in the axis of the impeller. The gas flow rate (Q_g) was regulated by using a manometer (Samson® 47 08-1155) and measured with a volumetric flow meter (Brooks® R2-25-C) with an accuracy of 0.05 L/min. Ranged from 0.33 to 3.33 L/min, these values remained quite narrow when compared to the available literature, they were initially imposed by the application underlying this work (namely the Autothermal Thermophilic Aerobic Digestion of sludge, see [19]). In terms of gas–liquid regime, it can be noticed (visual observations) that the operating conditions under test (N, Q_g, fluids) leaded to a complete dispersion regime, meaning thus that bubbles were almost uniformly distributed throughout the tank. One exception was for $N = 200$ rpm where the loading regime took place (presence of bubbles only in the upper part of the tank).

2.2. Methods of overall volumetric gas–liquid mass transfer coefficient measurement

2.2.1. Standard dynamic method

For implementing the standard dynamic method, the liquid phase was deoxygenated by flushing with nitrogen. Then, after replacing nitrogen by air, the variation in dissolved oxygen concentrations with time was measured until reaching the saturation. For that, two probes (InPro-6050, Mettler-Toledo®) and an acquisition card were implemented, as well as the LabView® software for data acquisition. The positions of the probes are represented in Fig. 1: they are located vertically at 4 cm and 18 cm above the bottom of the vessel, and horizontally at 1.5 cm from walls. Assuming a well mixed liquid phase, the mass balance in dissolved oxygen concentration is given by

$$\frac{dC_{O_2}}{dt} = K_l \cdot a \cdot (C^*_{O_2} - C_{O_2}) \tag{5}$$

where K_l is the overall mass transfer coefficient in the liquid side and a is the interfacial area between gas and liquid phases. The two-film theory of Lewis and Whitman [20] assumes that K_l is the result of two local mass transfer coefficients (k_l and k_g):

$$\frac{1}{K_l} = \frac{1}{k_l} + \frac{1}{m \cdot k_g} \tag{6}$$

where m is the Henry's constant ($m = H/P_s$). The solubility of oxygen is low: H is equal to 4.05×10^9 Pa (corresponding to $C^* = 9.09\ \mathrm{mg\,L^{-1}}$) in deionised water at 293 K in equilibrium with air under atmospheric pressure. So, all the resistance to oxygen mass transfer is located in the liquid film, leading to $K_l \approx k_l$.

As a consequence, the volumetric gas–liquid mass transfer coefficient, $k_l a$, can be directly deduced from the slope of the curve relating $\ln(C^*_{O_2} - C_{O_2})$ to time, obtained when integrating Eq. (5). The dynamics of the oxygen probe can be described using a first-order differential equation [21] as:

$$\frac{dC_p}{dt} = \frac{1}{t_p}(C_{O_2} - C_p) \tag{7}$$

where C_p is the dissolved oxygen concentration inside the probe. The time constant of the oxygen probe, t_p, was measured using a method based on probe response to negative oxygen steps [22] and found equal to 16 s. This latter value remained small when compared to mass transfer characteristic times, $1/k_l a$. As the temperature T_l slightly varied ($20 \pm 3\ ^\circ$C) with power dissipation, the usual temperature correction was applied [23]:

$$k_l a_{20} = k_l a_{T_l} \cdot 1.024^{(20 - T_l)} \tag{8}$$

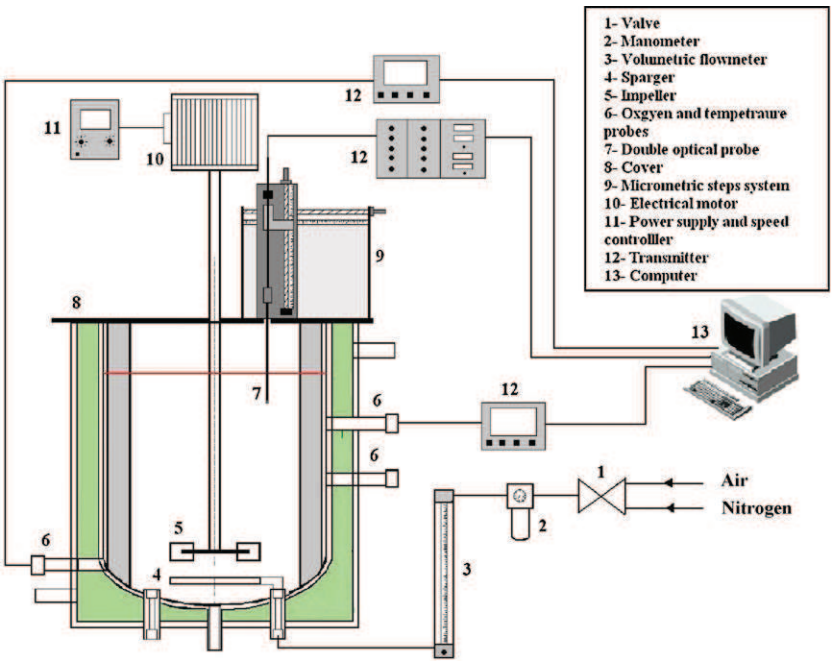

Fig. 1. Experimental set-up.

For a given operating condition (N and Q_g), the mean k_la in the tank was calculated by averaging the values measured by the two probes and for the three runs ($N' = 3$), such as:

$$k_la = < k_la > = \frac{1}{N'} \cdot \sum_{N'} \frac{|k_la_{top} + k_la_{bottom}|}{2} \quad (9)$$

The axial homogeneity (h) of volumetric gas–liquid mass transfer coefficients was also evaluated by using the criterion h defined as follows [24]:

$$h = \frac{1}{N''} \cdot \sum_{N''} \frac{|k_la_{top} - k_la_{bottom}|}{< k_la >} \quad (10)$$

where N'' was the number of experiments ($N'' = 60$ for each liquid phase).

2.2.2. Chemical method

When applying the latter dynamic method in viscous fluids, the impact of the probe dynamics and of the liquid film in front of the membrane on the probe can no more be ignored, as possibly biasing the measurements of k_la [25]. In addition, in such fluids, the gas hold-up structure is known to be very different from the one observed in water and other low-viscosity liquids: many tiny bubbles appear to accumulate during aeration and circulate with the liquid while large bubbles are also observed (bimodal bubble population). These tiny bubbles can actively contribute to mass transfer, depending whether they are in equilibrium with the level of dissolved solute in the liquid phase (high residence times) or not [26].

For these reasons, it has been chosen to implement a second method for k_la measurement. It will then enable to test the validity and accuracy of the dynamic method in the viscous fluids involved. This alternative method was the chemical method developed by [27], based on a mass balance on sodium sulphite (Na_2SO_3) concentrations during a given aeration time. Nitrogen was firstly injected into the liquid phase in order to eliminate the dissolved oxygen present in the tank. When the concentration of dissolved oxygen reached nearly zero, an adequate amount of Na_2SO_3 was introduced; air was then introduced in the tank and will react, during an aeration time $t_{aeration}$, with the small quantity of Na_2SO_3 introduced:

$$Na_2SO_3 + \frac{1}{2}O_2 \rightarrow Na_2SO_4 \quad (11)$$

The mass of Na_2SO_3 to initially introduce (m_t) must be chosen carefully, as it should enable to keep a zero oxygen concentration during the aeration time ($t_{aeration}$) while avoiding an excessive use of Na_2SO_3. Indeed, it is important to guaranty that the coalescing properties of the liquid phase were not affected by the presence of Na_2SO_3. A good compromise was to maintain an initial concentration below 0.5 g/L (i.e. $m_t < 3.5$ g with $V_l = 7.4$ L) [25]. Note that to minimize m_t, it was also possible to play on the aeration time ($t_{aeration}$), which was here typically ranged from 1.5 min to 9 min. The optimization of both m_t and $t_{aeration}$ was made easier by the fact that the orders of magnitude of k_La were known thanks to the measurements issued from the dynamic method.

When such conditions are respected, Painmanakul et al. [27] have shown that the overall volumetric gas–liquid mass transfer coefficient can be deduced from:

$$k_la = \frac{(1/2)(M_{O_2}/M_{Na_2SO_3}) \cdot (m_t - m_r)}{t_{aeration} \cdot V_l \cdot C^*_{O_2}} \quad (12)$$

where m_t is the total mass of Na_2SO_3 initially introduced, m_r is the mass of Na_2SO_3 remaining in the tank after an aeration period $t_{aeration}$, and $C^*_{O_2}$ is the concentration in dissolved oxygen at saturation. For glycerine solutions, $C^*_{O_2}$ was by default considered equal to 8.8 mg L^{-1} as in deionised water at 20 °C. An identical assumption was made for CMC and xanthan gum solutions in agreement with the data reported by [28] who showed that, in the range of concentrations here involved, no major variation of $C^*_{O_2}$ occurs when compared to water.

At last, for each condition, three samples (10 mL) were taken in the tank, immediately mixed with 10 mL of standard iodine reagent at 0.12 equiv./L. The titration of these samples with a sodium thiosulphate solution (0.05 equiv./L) and a starch indicator (iodometry titration) gave access to the concentration of Na_2SO_3 remaining in the tank after an aeration period $t_{aeration}$, and thus to m_r.

2.2.3. Surface- and volume-aerations

The overall volumetric gas–liquid mass transfer coefficient measured by the latter methods is in reality the global result of both contributions:

- *the surface-aeration*: it corresponds to the mass transfer occurring at the free surface which importance depends strongly on the surface motion. It also includes the aeration associated with the bubbles entrained from the surface into the liquid bulk;
- *the volume-aeration*: it is induced by the bubbles generated at the sparger directly inside the liquid bulk.

This can be expressed such as:

$$k_l a|_t = k_l a|_{surf} + k_l a|_{vol} \quad (13)$$

Some measurements are made with mechanical agitation and without bubbling at the sparger. They enable to get an idea of the relative importance of each contribution.

2.3. Fluids

The application underlying this study dealt with investigations on aeration performances in an Autothermal Thermophilic Aerobic Digestion (ATAD) process for treating sludge issued from waste water treatment plant [19]. As sludge was a very complex material, it was decided in a first step to work with model fluids instead of sludge. Their formulation was chosen so as to obtain rheological behaviours as close to sludge as possible, in particular in terms of shear-thinning properties. For these reasons, and with regard to literature, aqueous solutions of carboxymethylcellulose (CMC) and xanthan gum were selected. The use of two types of fluids offered the advantage to cover a wider range of combinations of flow and consistency indexes. To ensure their stability in time (during several days), NaCl was added at 0.1% (w/v) to the solutions of xanthan gum solutions [29] and $NaHCO_3$ (0.1 mol/L) + Na_2CO_3, $10H_2O$ (0.1 mol/L) to the solutions of CMC [30]. Various concentrations of CMC and xanthan gum were tested, and finally converged towards the following ones: 4 and 6 g/L for CMC, and 1 and 2 g/L for xanthan gum. In addition to these non-Newtonian fluids, deionised water and two aqueous solutions of glycerine (50% and 70%, v/v) were also chosen as Newtonian fluids.

The rheology of these fluids was measured, at 20 °C, by a rotational stress-controlled rheometrer (MCR500, PAAR Physica®) equipped a cone-plate device (50 mm in diameter, 3 degree in cone angle). Their density and surface tension were determined using a densimeter ERTCO® and a tensiometer involving the Wilhelmy plate method (3S GBX®). The physical and rheological properties of both Newtonian and non-Newtonian fluids are collected in Table 2.

The rheological behaviours of the non-Newtonian fluids were firstly characterised by measuring the variation of shear stress (τ) or apparent viscosity (μ_a) as a function of shear rates ($\dot{\gamma}$) which range varied from 0.1 to 3000 s^{-1}. When comparing the curves obtained for increasing and decreasing shear rates, no difference was observed whatever the non-Newtonian fluids: no hysteresis phenomenon then existed. Shown in Fig. 2, the rheograms obtained (issued from several trials) clearly illustrate the shear-thinning properties of these fluids. For each fluid, the yield stress was also determined, by applying the method proposed by [31] which consisted in oscillating stress sweep tests at a constant frequency (1 Hz); the dynamic yield stress was then defined at the end of the linear viscoelastic region, namely from the abscissa corresponding to the intersection point between the tangent to the plateau and the tangent to the inflexion point of the curve linking complex modulus and shear stress. Depending on the fluid, the yield stress

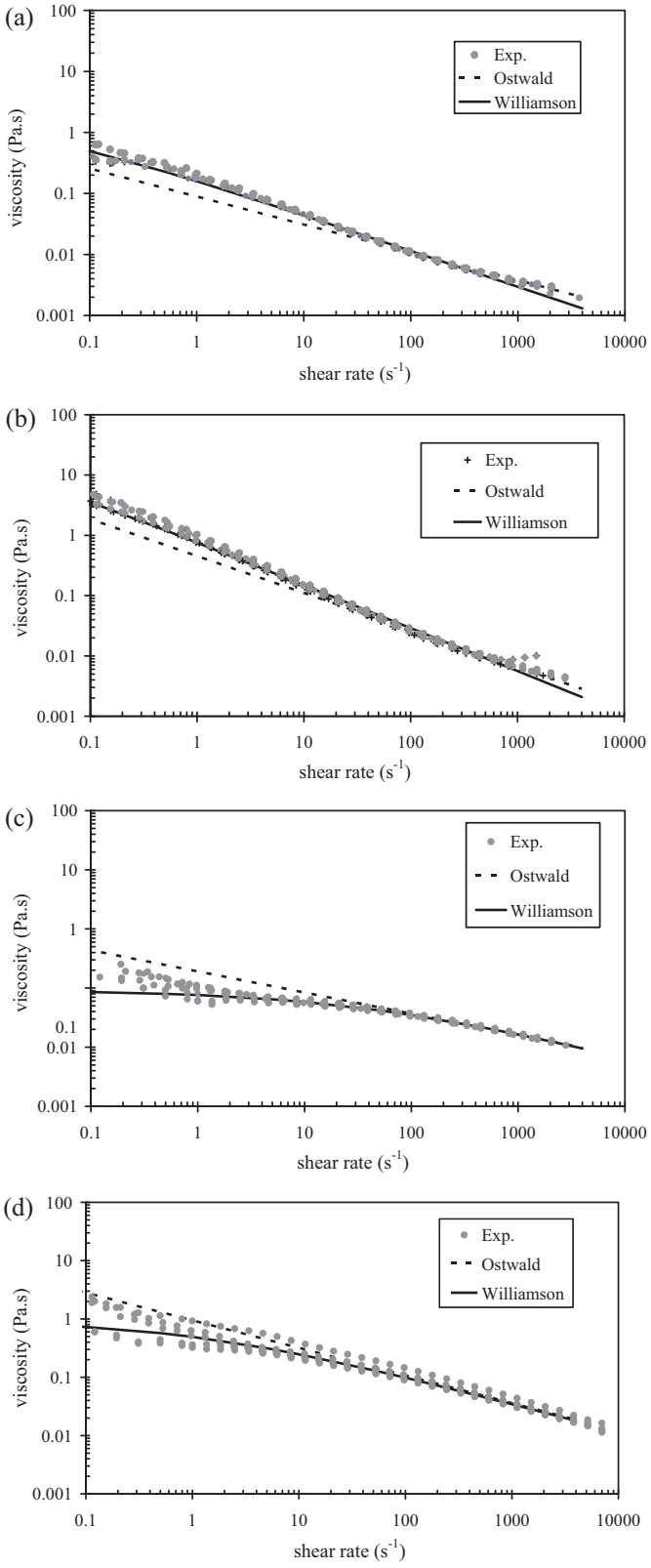

Fig. 2. Rheograms: (a) xanthan gum at 1 g/L, (b) xanthan gum at 2 g/L, (c) CMC at 4 g/L, and (d) CMC at 6 g/L.

was found to vary between 0.1 and 1 Pa, and remained thus negligible. To complete the rheological characterisation of the fluids, the viscoelastic properties were investigated, by means of creeping tests, relaxation tests and/or dynamic oscillating measurements. In

Table 2
Physical and rheological properties of the fluids.

	ρ_l (kg/m^3)	μ_l (Pa s)	σ (N/m)	Ostwald–de-Waele's model:		Williamson–Cross's model:		
				K (Pa s^n)	n_{ost}	μ_w (Pa s)	t_w (s)	n_w
Air	1.18	1.85×10^{-5}	–	–	–	–	–	–
Newtonian fluids								
Deionised water	998	0.001	0.0728	–	–	–	–	–
Glycerine 50% [Gly50]	1145	0.0109	0.0456	–	–	–	–	–
Glycerine 70% [Gly70]	1195	0.0349	0.0503	–	–	–	–	–
Non-Newtonian fluids								
CMC 4 g/L [CMC4]	997	–	0.0717	0.1914	0.642	0.091	0.029	0.546
CMC 6 g/L [CMC6]	1006	–	0.0771	0.9470	0.527	0.948	0.844	0.514
Xanthan gum 1 g/L [XG1]	1013	–	0.0753	0.0890	0.543	1.885	57.85	0.411
Xanthan gum 2 g/L [XG2]	1032	–	0.0767	0.5084	0.373	29.505	150.36	0.281

the range of shear rate investigated, no major elastic property was highlighted.

Based on these findings, some rheological models were chosen to mathematically describe the variation of apparent viscosity (μ_a) with shear rates ranging from 0.1 to 3000 s^{-1}. Among the large variability available in the literature, two models were selected:

- the Ostwald–de-Waele's model

$$\mu_a = K \cdot \dot{\gamma}^{n_{ost}-1} \tag{14}$$

where K and n_{ost} are respectively the consistency and flow indexes respectively.

- the Williamson–Cross's model

$$\mu_a = \frac{\mu_w}{1 + (t_w \cdot \dot{\gamma})^{1-n_w}} \tag{15}$$

where μ_w is a parameter describing a pseudo-Newtonian behaviour for the smallest shear rates, t_w is a time parameter characterizing the transition between the "pseudo-Newtonian" and purely shear-thinning behaviours, and n_w is the consistency index.

The values of K, n_{ost}, μ_w, t_w, n_w are reported in Table 2 for each fluid; they have been obtained by multi-parameter optimizations using the software Auto2fit®. In terms of consistency index, the most shear-thinning fluid appeared to be the solution of xanthan gum at 2 g/L. Based on the latter parameters, the apparent viscosities predicted by Eqs. (14) and (15) were compared to the experimental ones in Fig. 2. For all the fluids, a better agreement with experiments was obtained with the Williamson–Cross's model, insofar as it enables to describe the most faithfully possible the shape of the rheograms over the whole range of shear rates. This demonstrates that the fluids under test were not shear-thinning on the whole range of shear rates investigated, three parameters being required to well describe their behaviour.

3. Dimensional analysis for Newtonian and non-Newtonian Fluids

3.1. Generation of π_i-sets governing aeration process for Newtonian fluids

In the present stirred tank, bubbles were directly generating inside the liquid bulk by means of a gas sparger. Surface-aeration was of course present, but its contribution remained minor when compared to volume-aeration (see Section 4). Consequently, the overall volumetric gas–liquid mass transfer coefficient, k_la, can be considered as the tractable quantity which is significantly influenced by aeration conditions: it will be thus taken as target variable. Remind that such choice is based on the following relationship describing the physical absorption process according to the two-film theory:

$$\frac{G}{V_l} = k_l \cdot a \cdot \Delta C \quad \text{or} \quad k_l \cdot a = \frac{G}{V_l \cdot \Delta C} \tag{16}$$

where G/V_l is the mass throughput per unit volume of liquid and ΔC is a characteristic concentration difference. Eq. (16) implicitly assumes that (i) the intensity of gas–liquid contacting is so high that a quasi-uniform system is produced, (ii) the gas-phase mass coefficient k_g is negligible when compared to k_l (low soluble gases), (iii) the absorption rate at the interface is extremely fast, resulting in an equilibrium concentration of the dissolved gas at the interface C^* (e.g. $\Delta C = C^* - C$). Hence, the establishment of the list of parameters influencing the main parameter k_la should respect the following rules [7]: (i) k_la must be independent of all geometrical parameters (i.e. diameters of stirrer and tank, etc.), (ii) k_la must be independent of the material parameters of gas phase, and (iii) k_la is an intensive quantity because of its volume-related formulation.

As previously mentioned the number of the parameters influencing k_la, even performed in Newtonian liquids, is large and can be decomposed according to:

- The geometric parameters (see legend in Table 1), characterizing
  - the tank: T_t, H_l, curvature radius and angle (for tank's bottom), ...
  - the impeller: D, D_s, C, w, b, l, ...
  - the sparger: d, number, diameter and shape of holes, ...
- The material parameters:
  ρ_l, μ_l, ρ_g, μ_g, σ, $\mathcal{D}$, C^*
- The process parameters:

$$g, N, U_g = \frac{Q_g}{\pi \cdot T_t^2/4}, T_l, P_s, \ldots$$

Note that, in the present study, all the experiments were conducted at room temperature and atmospheric pressure, inducing thus that temperature and absolute pressure will not be listed. The geometry of the tank was also unchanged, as well as the type and position of both sparger and impeller. As a consequence, the list of individual physical quantities could be reduced: Table 3 shows the dimensional matrix obtained with the reduced list of relevant parameters.

It is voluntarily chosen to list the non-intensive parameters N and D instead of power per unit of liquid volume (P/V_l). The main motivation is that P/V_l is an intermediary variable which is not always available (in particular at industrial scale), and thus using such intensive variable would restrict the field of applications of the final dimensional correlation which will be established.

In Table 3, the columns are assigned to the individual physical quantities and the rows to the exponents appearing when

Table 3
Dimensional matrix of the influencing parameters (Newtonian fluids).

	Core matrix			Remnant matrix							
	ρ_g	μ_g	g	k_la	U_g	N	D	ρ_l	μ_l	σ	$\mathcal{D}$
Mass, M (kg)	1	1	0	0	0	0	0	1	1	1	0
Length, L (m)	−3	−1	1	0	1	0	1	−3	−1	0	2
Time, T (s)	0	−1	−2	−1	−1	−1	0	0	−1	−2	−1

each quantity is expressed as an appropriate power product of the base dimensions (mass, length, time). This table is structured in a core matrix and a residual matrix. The core matrix regroups the individual physical quantities put forward by the user to form the dimensionless ratios from other individual physical quantities (namely k_la, U_g, N, D, ρ_l, μ_l, σ, $\mathcal{D}$). Depending on the individual physical quantities assigned in the core matrix, several set of dimensionless numbers π_i can be obtained. It has been shown [32] that all the π_i-sets obtained from a single and identical relevance list are equivalent to each other from a point of view of dimensional analysis, and can be mutually transformed at leisure. The final form for the π_i-set should be laid down by the user so as to be the "best" suitable for evaluating and presenting the experimental data. Contrary to what commonly found in the literature, the gas properties ρ_g and μ_g (and not the liquid properties) were here chosen as individual physical quantities; the associated motivation was to generate dimensionless numbers dependent of a single influencing parameter, the gas phase being kept unchanged in this study (air).

Generating the set of dimensionless numbers (and possibly their future transformation) represents an extremely easy undertaking when compared to the drawing up of a reliable and as accurate as possible relevance list; this can be made by matrix transformation. The starting point consists in carrying out the so-called Gaussian algorithm in order to obtain a unit core matrix by linear transformations (zero-free main diagonal, beneath it zeros). Table 4 reports the unit core matrix associated with the dimensional matrix of Table 3. The analysis of the unit core matrix leads to the dimensionless ratios. Indeed, the rows of residual matrix are assigned to the exponents with whom the elements of the core matrix appear when the individual physical quantities of the residual matrix are expressed as an appropriate power product of the physical quantities of the core matrix. Literature [33] offers detailed examples of how to handle matrix transformation and recombination in order to quickly obtain the complete set of dimensionless numbers. This aspect will be then only briefly described in this paper. For Newtonian fluids, the matrix analysis leads to the eight dimensionless numbers, π_1 to π_8:

$$\pi_1 = \frac{k_la}{\rho_g^{1/3}\cdot\mu_g^{-1/3}\cdot g^{2/3}} \tag{17}$$

$$\pi_2 = \frac{U_g}{\rho_g^{-1/3}\cdot\mu_g^{1/3}\cdot g^{1/3}} \tag{18}$$

$$\pi_3 = \frac{N}{\rho_g^{1/3}\cdot\mu_g^{-1/3}\cdot g^{2/3}} \tag{19}$$

$$\pi_4 = \frac{D}{\rho_g^{-2/3}\cdot\mu_g^{2/3}\cdot g^{-1/3}} \tag{20}$$

$$\pi_5 = \frac{\rho_l}{\rho_g} \tag{21}$$

$$\pi_6 = \frac{\mu_l}{\mu_g} \tag{22}$$

$$\pi_7 = \frac{\sigma}{\rho_g^{-1/3}\cdot\mu_g^{4/3}\cdot g^{1/3}} \tag{23}$$

$$\pi_8 = \frac{\mathcal{D}}{\rho_g^{-1}\cdot\mu_g} \tag{24}$$

Note that π_1 is nothing other that the dimensionless volumetric mass transfer coefficient defined by [7], the combination of π_4 with $(\pi_3)^2$ leads to the Froude number, and π_8 is the inverse of a Schmidt number defined according to gas phase properties. By introducing the gas kinematic viscosity ($\upsilon_g = \mu_g/\rho_g$) and giving explicit notations, the latter numbers become:

$$\pi_1 = k_la^* = k_la\cdot\left(\frac{\upsilon_g}{g^2}\right)^{1/3} \tag{25}$$

$$\pi_2 = U_g^* = \frac{U_g}{(\upsilon_g\cdot g)^{1/3}} \tag{26}$$

$$\pi_3 = Fr = \frac{N^2\cdot D}{g} \tag{27}$$

$$\pi_5 = \rho^* = \frac{\rho_l}{\rho_g} \tag{28}$$

$$\pi_6 = \mu^* = \frac{\mu_l}{\mu_g} \tag{29}$$

$$\pi_7 = \sigma^* = \frac{\sigma}{(\rho_g^3\cdot\upsilon_g^4\cdot g)^{1/3}} \tag{30}$$

$$\pi_8 = Sc = \frac{\upsilon_g}{\mathcal{D}} \tag{31}$$

Thus, at a given temperature, under a given pressure, for the geometry of the aerated stirred tank under test (in particular for $H_l/T_t = 1$, $D/T_t = 0.4$, $D_s/T_t = 0.75$ and for the other geometrical ratios characteristics of the system), the dimensional analysis states that, when Newtonian fluids are involved, dimensionless volumetric mass transfer coefficient (k_la^*) is potentially affected by six dimensionless numbers, respectively describing the effects of superficial gas velocity, rotational impeller speed, liquid density, Newtonian viscosity, liquid surface tension and oxygen diffusivity:

$$k_la^* = f\left\{U_g^*, Fr, \rho^*, \mu^*, \sigma^*, Sc\right\} \tag{32}$$

Table 4
Unit core matrix obtained by linear transformations of dimensional matrix (Newtonian fluids).

	Core matrix			Residual matrix							
	ρ_g	μ_g	g	k_la	U_g	N	D	ρ_l	μ_l	σ	$\mathcal{D}$
$M+T+2A$	1	0	0	$\frac{1}{3}$	$-\frac{1}{3}$	$\frac{1}{3}$	$-\frac{2}{3}$	1	0	$-\frac{1}{3}$	−1
$3M+L+T+A$	0	1	0	$-\frac{1}{3}$	$\frac{1}{3}$	$-\frac{1}{3}$	$\frac{2}{3}$	0	1	$\frac{4}{3}$	1
$A = -\frac{1}{3}\times(3M+L+2T)$	0	0	1	$\frac{2}{3}$	$\frac{1}{3}$	$\frac{2}{3}$	$-\frac{1}{3}$	0	0	$\frac{1}{3}$	0

Such formulation of dimensionless numbers offers the advantage to enable the impact of all influencing parameters to be studied separately, or in others words each dimensionless number is defined for a single influencing variable. This is not the case in the literature where, for example, most of the authors used the aeration number, $Na = Fl_g = Q_g/(N \cdot D^3)$, in which the effect of gas flow rate is not decoupled from the one of rotational impeller speed.

At this state, the dependence of Eq. (32) is all that can be contributed by the theory of similarity. The mathematical expression for the function *f*, namely for the process relationship, has to be determined experimentally.

3.2. Extension of the theory of similarity to the cases of variable material properties

When using the dimensional analysis to model system answers, it is generally assumed that the material properties remain unaltered in the course of the process. However, the invariability of material properties cannot be assumed when non-Newtonian fluids are involved. Indeed, at the least one of the material properties, the apparent viscosity, can no longer be considered as a constant inside the whole volume of the aerated stirred tank, insofar as the dependency of this latter with the shear rates ($\dot{\gamma}$) generates a spatial distribution of the liquid viscosity. The underlying question addressed to the dimensional analysis is now: *how must the space of dimensionless numbers, π_i, be built in presence of such variable material property*?

In the case of materials with constant properties, no special precaution should be made to guarantee that a process relationship correlating a set of dimensionless ratios is also applicable to another material. This is not true for materials with variables properties, as demonstrated by [34]. In this case, we should first ensure as priority that a certain similarity exists for materials in order to extend the range of validity of the process relationship to other materials. Despite that, the theory of similarity has little changed since its beginning, and the dimensional modelling involving materials with variable physical properties remains treated, in most of the papers, as the case with constant material properties. The authors ignore then the fact that the spatio-temporal variability of material properties influences the course of the process! One exception is the modelling of the transformation processes where a material having a temperature-dependence in viscosity is submitted to heat transfer condition. Most of attempts made to take into account the variability of product properties in the reactor have consisted in adding a new ratio raised to a certain exponent to characterize the system response. This ratio is defined by the ratio between the viscosities at bulk temperature and at wall temperature. However, this kind of enlargement of the set of dimensionless ratios is theoretically valid only for few limited cases, that is to say only if the material function (here viscosity versus temperature) satisfies specific criteria [34]. In other words, such method leads to biased predictions and thus, cannot be generalised when handling other fluids. Despite this fact, this ratio remains systematically used, whatever the products investigated, in most of the studies since [35].

The theoretically consistent way of proceeding has been introduced by Pawlowski in 1971 [34] and remembered by [32,36]. The method consists in introducing some additional parameters in the relevance list so as to take into account the variation in the flow domain of the physical property, noted *s* (for example viscosity), as a function of a parameter noted *p* (for example temperature or shear rate); $s(p)$ is called the *material function* (for example $\mu(T)$ or $\mu(\dot{\gamma})$). This implies that the π_i-space governing the process will be extended in comparison to fluids having constant properties. The guidelines to introduce the right number of additional dimensional parameters are detailed in [34]. Hence, when dealing with a material function $s(p)$ which is apparent viscosity $\mu_a(\dot{\gamma})$, the Pawlowski's work [34] can be summed up, as follows:

- Firstly, all the dimensional parameters defined in the relevant list with fluids having constant properties (Newtonian case) should be conserved, except for the variable physical properties in question (here apparent viscosity $\mu_a(\dot{\gamma})$).
- Secondly, the Newtonian viscosity should be replaced by a reference apparent viscosity, μ_o, calculated at a *reference shear rate*, $\dot{\gamma}_o$. It is important to point out that any value for the reference shear rate can be chosen.
- Thirdly, the reference shear rate should be added in the list of relevant parameters. At this stage, we can point out that some exceptions to this rule exist. Indeed, it has been demonstrated that adding the reference point is not necessary when the material function $s(p)$, here $\mu_a(\dot{\gamma})$, can be described by the following family of curves:

$$s(p) = (A + B \cdot p)^C \quad \text{or} \quad s(p) = \exp(A + B \cdot p) \tag{33}$$

  where *A*, *B* and *C* are three independent constants.
- Finally, a set of additional dimensionless numbers should be added in the relevant (dimensional) list to take into account the dependency of material function. These dimensionless parameters, called π_{rheol}, correspond to all the dimensionless ratios π_i which appear in the expression of the function *u*, except for the ratio $\dot{\gamma}/\dot{\gamma}_0$:

$$\{\pi_{rheol}\} = \left\{ \{\pi_i\} \text{ such as } u = (\dot{\gamma} - \dot{\gamma}_0)\frac{1}{\mu_a(\dot{\gamma}_0)} \cdot \left[\frac{d\mu_a}{d\dot{\gamma}}\right]_{\dot{\gamma}=\dot{\gamma}_o} = g\left(\frac{\dot{\gamma}}{\dot{\gamma}_0}; \{\pi_i\}\right) \right\} \tag{34}$$

When integrating the previous guidelines, the list of the influencing parameters established for Newtonian fluids becomes for non-Newtonian fluids:

$$\{k_l a, \rho_g, \mu_g, g, U_g, N, D, \rho_l, \sigma, \mathcal{D}, \mu_a(\dot{\gamma}_o), \dot{\gamma}_o, \pi_{rheol}\} \tag{35}$$

The next step is to find the type of material function describing the rheological behaviour of viscous fluids having shear-thinning properties. As presented in Section 2, two models are well adapted for the investigated fluids: the Ostwald–de-Waele's model (Eq. (14)) and the Williamson–Cross's model (Eq. (15)). As these models are able to describe the variation of viscosity with shear rate for all the aqueous solution of CMC and xanthan gum, each of them constitute one possible material function.

3.2.1. Case No. 1: Ostwald–de-Waele's model.

When the material function corresponds to the Ostwald–de-Waele's model, the function *u* can be expressed as:

$$u = \left(\frac{\dot{\gamma}}{\dot{\gamma}_0} - 1\right)(n_{ost} - 1) \tag{36}$$

Consequently,

$$\{\pi_{rheol}\} = \{n_{ost}\} \tag{37}$$

The Ostwald–de-Waele's model, defining as $\mu_a = K \cdot \dot{\gamma}^{n_{ost}-1}$ (Eq. (14)), verifies Eq. (33), implying thus that the reference shear rate, $\dot{\gamma}_o$, can be removed from the relevance list. As a consequence, for purely viscous fluids having shear-thinning properties, the additional parameters is restricted to n_{ost} and the Newtonian viscosity is replaced by $\mu_a(\dot{\gamma}_o)$. Eq. (32) established for Newtonian fluids becomes then:

$$k_l a^* = g\left\{U_g^*, Fr, \rho^*, \sigma^*, Sc, \mu^* = \frac{\mu_a(\gamma_o)}{\mu_g}, n_{ost}\right\} \tag{38}$$

Table 5
Dimensional results for k_la (expressed in s^{-1}): Newtonian and non-Newtonian fluids.

N (rpm)	Q_g (L/min)	Newtonian fluids		Non-Newtonian fluids				
		Water	Gly50	Gly70	CMC4	CMC6	XG1	XG2
200	0.33	9.05×10^{-4}	–	–	–	–	–	–
	0.9	1.91×10^{-3}	–	–	–	–	–	–
	1.6	3.35×10^{-3}	7.75×10^{-4}	3.13×10^{-4}	1.64×10^{-3}	1.26×10^{-3}	1.55×10^{-3}	1.31×10^{-3}
	2.33	4.58×10^{-3}	1.05×10^{-3}	4.22×10^{-4}	2.08×10^{-3}	1.85×10^{-3}	2.06×10^{-3}	1.47×10^{-3}
	3	5.33×10^{-3}	1.45×10^{-3}	5.15×10^{-4}	2.58×10^{-3}	2.01×10^{-3}	2.68×10^{-3}	2.16×10^{-3}
	3.33	5.88×10^{-3}	1.77×10^{-3}	5.75×10^{-4}	2.82×10^{-3}	2.3×10^{-3}	2.85×10^{-3}	2.56×10^{-3}
400	0.33	2.31×10^{-3}	–	–	–	–	–	–
	0.9	4.91×10^{-3}	–	–	–	–	–	–
	1.6	8.69×10^{-3}	2.90×10^{-3}	6.82×10^{-4}	3.68×10^{-3}	2.54×10^{-3}	4.83×10^{-3}	3.61×10^{-3}
	2.33	1.12×10^{-2}	3.50×10^{-3}	8.00×10^{-7}	4.43×10^{-3}	4.40×10^{-3}	5.93×10^{-3}	4.81×10^{-3}
	3	1.29×10^{-2}	4.28×10^{-3}	9.99×10^{-4}	4.98×10^{-3}	4.98×10^{-3}	6.59×10^{-3}	6.51×10^{-3}
	3.33	1.31×10^{-2}	4.63×10^{-3}	1.19×10^{-3}	5.19×10^{-3}	5.53×10^{-3}	$7 \times 10 \times 10^{-3}$	8.01×10^{-3}
600	0.33	4.30×10^{-3}	–	–	–	–	–	–
	0.9	9.19×10^{-3}	–	–	–	–	–	–
	1.6	1.62×10^{-2}	4.72×10^{-3}	1.38×10^{-3}	7.51×10^{-3}	3.99×10^{-3}	9.52×10^{-3}	7.68×10^{-3}
	2.33	1.82×10^{-2}	5.73×10^{-3}	1.77×10^{-3}	8.60×10^{-3}	6.90×10^{-3}	1.13×10^{-2}	9.57×10^{-3}
	3	2.06×10^{-2}	6.39×10^{-3}	2.25×10^{-3}	9.23×10^{-3}	8.20×10^{-3}	1.30×10^{-2}	1.11×10^{-2}
	3.33	2.26×10^{-2}	6.78×10^{-3}	2.55×10^{-3}	9.44×10^{-3}	9.05×10^{-3}	1.39×10^{-2}	1.20×10^{-2}
800	0.33	4.94×10^{-3}	–	–	–	–	–	–
	0.9	1.39×10^{-2}	–	–	–	–	–	–
	1.6	2.26×10^{-2}	6.87×10^{-3}	2.35×10^{-3}	1.14×10^{-2}	6.40×10^{-3}	1.29×10^{-2}	1.08×10^{-2}
	2.33	2.68×10^{-2}	7.61×10^{-3}	3.31×10^{-3}	1.32×10^{-2}	8.30×10^{-3}	1.51×10^{-2}	1.28×10^{-2}
	3	2.81×10^{-2}	8.14×10^{-3}	3.97×10^{-3}	1.45×10^{-2}	9.17×10^{-3}	1.79×10^{-2}	1.43×10^{-2}
	3.33	3.21×10^{-2}	8.45×10^{-3}	4.46×10^{-3}	1.48×10^{-2}	9.75×10^{-3}	1.87×10^{-2}	1.57×10^{-2}
1000	0.33	1.05×10^{-2}	–	–	–	–	–	–
	0.9	1.43×10^{-2}	–	–	–	–	–	–
	1.6	2.25×10^{-2}	8.36×10^{-3}	4.41×10^{-3}	1.54×10^{-2}	8.90×10^{-3}	1.70×10^{-2}	1.38×10^{-2}
	2.33	2.70×10^{-2}	8.87×10^{-3}	5.21×10^{-3}	1.75×10^{-2}	1.05×10^{-2}	2.06×10^{-2}	1.68×10^{-2}
	3	2.84×10^{-2}	9.18×10^{-3}	5.74×10^{-3}	1.88×10^{-2}	1.17×10^{-2}	2.36×1010^{-2}	1.89×10^{-2}
	3.33	3.34×10^{-2}	9.48×10^{-3}	6.21×10^{-3}	1.90×10^{-2}	1.29×10^{-2}	2.61×10^{-2}	2.06×10^{-2}

When degenerated to the Newtonian case, the material function associated with the Ostwald–de-Waele's model leads to $n_{ost} = 1$ and $\mu^* = \mu_a/\mu_g$ where $\mu_a = \mu_l$ is the Newtonian viscosity.

3.2.2. Case No. 2: Williamson–Cross's model

When the material function corresponds to the Williamson–Cross's model, the function u can be expressed as:

$$\mu = \left(\frac{\dot\gamma - \dot\gamma_0}{\dot\gamma_0}\right) \cdot \frac{(n_w - 1)\cdot(t_w \cdot \dot\gamma_0)^{(-n_w)}}{1 + (t_w \cdot \dot\gamma_0)^{1-n_w}} \tag{39}$$

Consequently,

$$\{\pi_{rheol}\} = \{n_w, t_w \cdot \dot\gamma_0\} \tag{40}$$

The reference shear rate, $\dot\gamma_o$, should be listed as the Williamson–Cross's model does not verify Eq. (33). Finally, the new variables to add in the relevant dimensional list are:

$$\{\dot\gamma_o, n_w, t_w \cdot \dot\gamma_0\} \tag{41}$$

Nevertheless, as $\dot\gamma_o$ can theoretically take any value, it is possible to choose:

$$\dot\gamma_o = \frac{1}{t_w} \tag{42}$$

By this way, the supplementary variables are restricted to:

$$\{t_w, n_w\} \tag{43}$$

As a consequence, for the fluids described by the Williamson–Cross's model, the additional parameters are t_w and n_w, and the Newtonian viscosity should be replaced by

$$\mu_a\left(\frac{1}{t_w}\right) = \mu_0 = \frac{\mu_w}{2} \tag{44}$$

After introducing these variables in the core matrix (Table 3) and applying the linear transformations from Table 4, the set of dimensionless numbers defining aeration process is enlarged by two dimensionless numbers:

$$\pi_9 = n_w \quad \text{and} \quad \pi_{10} = t_w^* = \frac{1}{t_w} \cdot \left(\frac{\upsilon_g}{g^2}\right)^{1/3} \tag{45}$$

Eq. (32) established for Newtonian fluids becomes then:

$$k_la^* = h\left\{U_g^*, Fr, \rho^*, \sigma^*, Sc, \mu^* = \frac{\mu_a(1/t_w)}{\mu_g}, n_w, t_w^*\right\} \tag{46}$$

Note that the Williamson–Cross's model leads to a Newtonian behaviour for particular values of n_w and t_w : namely $n_w = 1$ and $t_w = 1$. In this case, $\mu_l = \mu_w/2$.

4. Results

4.1. Validation of k_la measurements

In Table 5 are collected the set of experiments which will serve as database for the dimensional analysis. It is constituted by 150 measures of k_la (including 70 values for the Newtonian case), carried out at five rotational impeller speeds ($200 \le N \le 1000$ rpm) and four flow rates ($0.33 \le Q_g \le 3.33$ L/min), and for several fluids (three Newtonian fluids, four non-Newtonian fluids). Note that these overall volumetric mass transfer coefficients correspond to the values obtained with the dynamic method, and averaged from the measures for both probes and three runs (Eq. (9)).

Whatever the fluids, the criterion for axial homogeneity (defined in Eq. (10)) has been found varying from 6 to 8% for $N = 200$ rpm, and from 1 to 3% for $N = 1000$ rpm [19,37], the smallest value being obtained for the probe located at the top of the tank. Then, no significant spatial heterogeneity takes place in the tank, and these values of k_la can be considered representative of the aeration state in the whole tank.

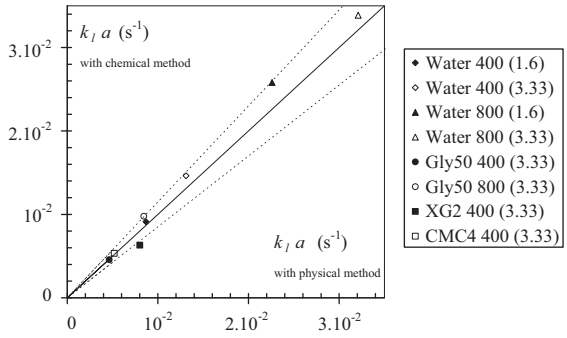

Fig. 3. Comparison between chemical and physical methods for measuring $k_l a$ (the dotted lines correspond to a deviation of ±15%; in the legend, the first number is N in rpm, the number into brackets Q_g in L/min).

Fig. 3 presents, for some representative cases, a comparison between the physical and chemical methods for measuring $k_l a$. A good agreement between both methods is observed: the deviation never exceeds 15% which corresponds to the order of magnitude associated with the experimental uncertainty in the chemical method [27]. As a consequence, the values of $k_l a$ reported in Table 5 can be assumed relevant as validated by two methods.

The contribution of surface aeration to the overall volumetric gas–liquid mass transfer coefficient has been estimated by measuring $k_l a$ without bubbling at the ring sparger (see Section 2). For $200 \leq N \leq 1000$ rpm and $1.6 \leq Q_g \leq 3.33$ L/min, the following trends have been obtained [37]:

- for water, $k_l a\big|_{surf} < 0.14 \times k_l a\big|_t$,
- for glycerine at 50%, $k_l a\big|_{surf} < 0.15 \times k_l a\big|_t$, and for glycerine at 70%, $k_l a\big|_{surf} < 0.23 \times k_l a\big|_t$,
- for CMC at 4 g/L, $k_l a\big|_{surf} < 0.08 \times k_l a\big|_t$, and for CMC at 6 g/L, $k_l a\big|_{surf} \ll k_l a\big|_t$,
- for xanthan gum at 1 g/L, $k_l a\big|_{surf} < 0.17\, k_l a\big|_t$, and for xanthan gum at 2 g/L $k_l a\big|_{surf} < 0.14 \times k_l a\big|_t$.

This demonstrates that the surface aeration remains small when compared to volume aeration, confirming thus that $k_l a|_t$ is the adequate target parameter to tract in the dimensionless analysis for qualifying the aeration state in the tank.

When analysed in detail [19], Table 5 points that, for a given fluid, the overall volumetric mass transfer coefficients logically increase for increasing rotational impeller speeds and gas flow rates. The relative contributions of gas sparging (Q_g) and mechanical agitation (N) on the variations of $k_l a$ are comparable, even if the rotational impeller speed plays a more pronounced role. The present investigations are then performed under the intermediary condition defined by [13,14], namely the condition ranged between the bubbling-controlling condition (at relatively high gas flow rates) and the agitation-controlling condition (at relatively high rotational impeller speeds). More important is the major reduction in $k_l a$ observed in presence of viscous fluids (Newtonian and non-Newtonian) when compared to water. To better appreciate this phenomenon, the following ratio can be defined:

$$R = \frac{k_l a|_{viscous\,fluid}}{k_l a|_{water}} \tag{47}$$

For instance, at Q_g = 3 L/min and for $200 \leq N \leq 1000$ rpm, the latter ratio R varies:

- from 27 to 32% in glycerine at 50%, and from 9.7 to 20% in glycerine at 70%,
- from 43 to 66% in CMC at 4 g/L, and from 38 to 43% in CMC at 6 g/L,
- from 50 to 83% in xanthan gum at 1 g/L and from 40 to 66% in xanthan gum at 2 g/L.

The comparison of such values of $k_l a$, or any other attempts for their modelling, is usually made (see Section 1) by calculating the apparent viscosity basing on the well-known concept of Metzner–Otto and the Ostwald–de-Waele's model (Eq. (14)). When applying this method [19], it is possible neither to explain nor to understand satisfactorily these results, confirming thus the requirement to perform more consistent investigations on the influencing parameters.

4.2. Dimensionless results for Newtonian fluids

The oxygen diffusivity, $\mathcal{D}$, was unknown for the viscous Newtonian and non-Newtonian fluids under test. Indeed, such information remains unavailable in the literature, and the usual correlations (for example the Wilke–Chang one) cannot be applied by lack of some required data (for example the association factor of solvent). So, the contribution of Schmidt number in the process relationship (Eq. (32)) cannot be rigorously sought. By default, whatever the liquid phases, the oxygen diffusivity, $\mathcal{D}$, will be assumed equal to the one in water at 20 °C (i.e. to 2×10^{-9} m s^{-2}). In this case, the Schmidt number Sc (defined with respect to *gas* cinematic viscosity, Eq. (31)) is then equal to 7850. As a consequence, it seems reasonable to assert that the process relationship established will be insured for values of Schmidt numbers close to this latter. In addition, the variation of density for the fluids investigated is not important (Table 2), implying thus that the change in ρ^* is weak ($847 < \rho^* < 1015$). As a consequence, for securing the process relationship, it is chosen to ignore the possible alterations of ρ^* and Sc in Eq. (32), leading to:

$$k_l a^* = f'\{U_g^*, Fr, \mu^*, \sigma^*\} \tag{48}$$

Having no mechanistic indication on the form of the f'-relation, the simplest monomial form is looked for:

$$k_l a^* = \alpha \cdot (Fr)^a \cdot (U_g^*)^b \cdot (\mu^*)^c \cdot (\sigma^*)^d \tag{49}$$

where α, a, b, c and d are respectively the constant and the exponents to which the dimensionless Froude, gas velocity, viscosity and surface tension numbers are raised. The dimensionless viscosity, μ^*, is calculated using the Newtonian viscosity (μ_l) reported in Table 2. The software Auto2fit® is used to perform the multi-parameter optimization required to determine α, a, b, c and d. Different mathematical algorithms are systematically tested (global Levenberg–Marquardt, global Quasi-Newton, standard differential evaluation, genetic algorithm) to verify the stability of the results and their independency with initial conditions. The mean standard deviation is calculated from:

$$\varepsilon = \frac{1}{N} \sum_{i=1,N} \left| \frac{(k_l a)^*_{exp,i} - (k_l a)^*_{mod,i}}{(k_l a)^*_{exp,i}} \right| \tag{50}$$

In a first time, it is interesting to visualize the effect of Newtonian viscosity (μ^*) on $(k_l a)^*$ separately from the other variables. The problem is that the graphic representation associated with Eq. (49) requires five dimensions as $(k_l a)^*$ depends on Fr, U_g^*, μ^* and σ^*. A simple way to sidestep this problem is to come down to a 2D representation, in which the impact of σ^* on $(k_l a)^*$ is neglected and an identical exponent is imposed for the Froude and dimensionless superficial gas velocity numbers. This is illustrated in Fig. 4, where $(k_l a)^*$ is plotted as a function of $(U_g^* \cdot Fr)^{2/3}$ for Newtonian fluids. The value of 2/3 is chosen as a first approximation for the exponent

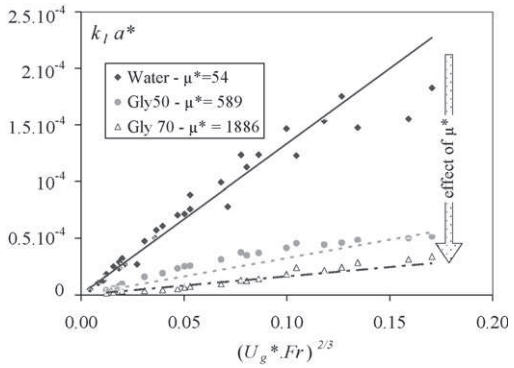

Fig. 4. Effect of dimensionless Newtonian viscosity, $k_l a^* = k_l a \cdot (\upsilon_g / g^2)^{1/3}$, versus $(U_g^* \cdot Fr)^{2/3}$ (the dotted/continuous lines correspond to the values predicted by Eq. (51)).

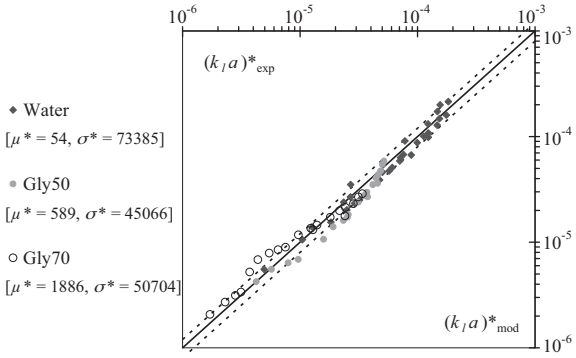

Fig. 5. Experimental dimensionless overall gas–liquid mass transfer coefficient versus $k_l a^*$ predicted from Eq. (52) (Newtonian fluids). The dotted lines correspond to a deviation of ±20%.

on Fr and U_g^*, as already encountered in the literature (see review of [3]). Thus, Fig. 4 offers the advantage to easily appreciate the negative effect of μ^* on aeration performances: whatever $(U_g^* \cdot Fr)^{2/3}$, an increase of μ^* from 54 (water) to 1886 (glycerine 70%) leads to a drastic reduction of $(k_l a)^*$ (more than 85%).

When imposing the exponent 2/3 to $(U_g^* \cdot Fr)$, the best fitting between experimental data and Eq. (49) without taking into account σ^* leads to:

$$k_l a^* = 0.1420 \cdot (Fr \cdot U_g^*)^{2/3} \cdot (\mu^*)^{-0.591} \tag{51}$$

The associated mean standard deviation is equal to 17.1%. To test the robustness of such correlation (in particular of the exponents found), several cases are now tested when implementing the multi-parameter optimization:

- Case No. 1: all the exponents in Eq. (49) are kept free and σ^* is neglected;
- Case No. 2: the exponents of Fr and of U_g^* are imposed identical without any specified value, and σ^* is neglected;
- Case No. 3: the exponents of Fr and U_g^* are imposed equal to 2/3 (as in Eq. (51)), but now the effect of σ^* is taken into account.

In Table 6 are collected, for each case, the constant and exponents of Eq. (49) deduced from the multi-parameter optimization. In a general point of view, no major difference appears between the different cases: the exponent of μ^* remains close to −0.59 (deviation < 1.3%), and the exponents of Fr and U_g^* do not vary significantly whether they are imposed identical or not (deviation < 6.5%). These findings confirm that the orders of magnitude of the exponents found in Eq. (51) are relevant, and thus, that this correlation is mathematically robust. Note that, even if Fr and U_g^* have the same exponent, the contribution of N is two times higher than the one of superficial gas velocity, as the Froude number is expressed in squared rotational impeller speed (Eq. (27)); this is coherent with these observations made on the dimensional results (Section 4.1). The cases No. 1 and No. 2 leads to a slight improvement (smaller than 1%) of the mean standard deviation (ε); however, the exponents of Eq. (51) will be thereafter conserved, insofar as they lead to the most simple formulation, and also as the value of 2/3 is already encountered in the literature. Based on that, the effect of surface tension, $\sigma^* = \sigma/(\rho_g^3 \cdot \upsilon_g^4 \cdot g)^{1/3}$, has been added in Eq. (51) (Case No. 3): the constant is in return increased and a negative exponent appears for σ^* (−0.245). This latter logically confirms the positive impact of decreasing surface tension on aeration: when surface tension is reduced (for example when adding surfactant or alcohol in the liquid phase), smaller bubble sizes are generated, leading to a rise in interfacial area and thus in overall volumetric mass transfer coefficient. In the literature [7], this usually results in positive exponents for the Weber number.

Table 6
Dimensionless modelling for Newtonian fluids using Eq. (49) (in bold the case retained).

Case	α	a	b	c	d	ε (%)
No. 1	0.02125	0.747	0.66	−0.605	–	*16.1*
No. 2	0.01535	0.683	0.683	−0.592	–	*16.8*
No. 3	**0.2097**	**2/3**	**2/3**	**−0.591**	**−0.245**	***16.8***

At last, at a given temperature, under a given pressure, for the geometry of the aerated stirred tank under test (in particular for $H_l/T_t = 1$, $D/T_t = 0.4$, $D_s/T_t = 0.75$ and for the other geometrical ratios characteristics of the system), the dimensional analysis states that the process relationship for Newtonian fluids is expressed by:

$$k_l a^* = 0.2097 \cdot (Fr \cdot U_g^*)^{2/3} \cdot (\mu^*)^{-0.591} \cdot (\sigma^*)^{-0.245}$$
$$\text{valid for} \begin{cases} 0.096 < Fr < 2.4, \quad 0.0029 < U_g^* < 0.029, \quad 54 < \mu^* < 1886 \\ 847 < \rho^* < 1015, \quad 50704 < \sigma^* < 73385, \quad Sc = 7850 \end{cases} \tag{52}$$

Fig. 5 compares the experimental data with the dimensionless overall volumetric gas–liquid mass transfer coefficients predicted by Eq. (52). A good agreement is observed, as the mean standard deviation remains smaller than 17%. It can been observed that some data corresponding to the smallest $k_l a^*$ (obtained for low speeds in glycerine) tends to move away from the straight lines representing $(k_l a^*)_{exp} = \pm 20\% \cdot (k_l a^*)_{pred}$. This should be linked to the fact that, in such conditions, the gas–liquid regime corresponds to a loading regime, and not to a complete dispersion regime characterizing all the other operating conditions. The mechanical agitation is not then sufficient to disperse uniformly the bubbles in the whole volume of tank, in particular in the lower part of the tank (below the impeller). Hence, the relative contributions of the mechanisms controlling $k_l a$ (mechanical agitation against sparger aeration) deviates from the ones acting when a complete dispersion regime takes place. When such changes in regime occurs, it becomes then difficult to define an unique *and* accurate process relationship able to describe the entire range of operating conditions. Some deviations can be also observed for the highest vales of $k_l a$; they can be here associated with an increasing contribution of the surface aeration (mass transfer occurring at the free liquid surface) when rotational impeller speed rises. Indeed, for the highest N, a significant vortex appears in the centre of the tank and entrains many bubbles. In such conditions, the mechanism (or regime) of aeration is deviated to a pure volume-aeration, and thus, the choice of $k_l a\big|_t$ (and not $k_l a\big|_{surf}$) for tracting volume-aeration state is less representative.

To conclude, it should be kept in mind that the validity of Eq. (52) can be at present guaranteed only in the range of dimensionless

Table 7
Dimensionless numbers characteristics for liquid properties.

	ρ^*	σ^*	n_{ost}	μ^*_{ost}	n_w	t^*_w	μ^*_w
Water	848	73385	1	54	1	1	108
Gly50	973	45966	1	589	1	1	1178
Gly70	1015	50704	1	1886	1	1	3773
CMC4	861	75905	0.642	1866	0.546	0.201	4944
CMC6	877	77316	0.527	5309	0.513	6.84×10^{-3}	5.12×10^{4}
XG1	847	72276	0.543	539	0.411	9.98×10^{-5}	1.02×10^{5}
XG2	855	77719	0.373	1366	0.281	3.84×10^{-5}	1.59×10^{6}

numbers above mentioned, at given temperature and pressure, and in the geometry defined in Section 2.

4.3. Dimensionless results for non-Newtonian fluids

4.3.1. When considering the model of Ostwald–de-Waele

As any value can be considered (see Section 3.2), the reference shear rate, $\dot{\gamma}_o$, has been arbitrary chosen equal to 120 s^{-1}. The dimensionless numbers describing the rheological properties associated with the Ostwald–de-Waele's model (Table 2) and such $\dot{\gamma}_o$ are collected in Table 7 (fourth and fifth columns). It can be logically observed that the flow index (n_{ost}) decreases when increasing the concentration, the smallest value being obtained for the most concentrated solution of xanthan gum. Dimensionless apparent viscosity (μ^*_{ost}) are higher for aqueous solutions of CMC than the ones of xanthan gum.

Basing on the reasons mentioned in the case of Newtonian fluids, the possible changes in ρ^* and in Sc will be neglected in Eq. (38) previously established when the model of Ostwald–de-Waele is considered. Thus, Eq. (38) becomes:

$$k_l a^* = g' \left\{ U_g^*, Fr, \sigma^*, \mu^* = \frac{\mu_a(\gamma_o)}{\mu_g}, n_{ost} \right\} \tag{53}$$

The simplest monomial form is here also looked for the g'-relation (no mechanistic information available):

$$k_l a^* = \alpha' \cdot (Fr)^{a'} \cdot (U_g^*)^{b'} \cdot (\mu^*)^{c'} \cdot (\sigma^*)^{d'} \cdot (n_{ost})^{e} \tag{54}$$

where α', a', b', c', d' and e are respectively the constant and the exponents to which the dimensionless Froude, superficial gas velocity, viscosity, surface tension and flow index numbers are raised (Auto2fit®). However, it is important to keep in mind that the modelling for Newtonian fluids is a degraded case of the one for non-Newtonian fluids. As a consequence, the exponents of Fr, U_g^*, μ^* and σ^* (namely a', b', c', d') are already defined, and will be thus taken equal respectively to 2/3, 2/3, −0.591 and −0.245 as in the Newtonian case (Table 6, Case No. 3).

In Fig. 6, $(k_l a)^*$ is plotted as a function of $(U_g^* \cdot Fr)^{2/3}$ for all the fluids. Such figure is particularly important as the effects of μ^* and n_{ost} can be visualized separately. Indeed, at a given μ^*, an decrease in n_{ost} clearly induces an increase in $(k_l a)^*$, or in other words, the shear-thinning character of fluids favours the aeration performances, probably due to the spatial heterogeneity of viscosity. This is illustrated when comparing either (i) the glycerine at 70% and the aqueous solutions of CMC at 4 g/L which have almost the same dimensionless apparent viscosity (1886 against 1866), but different flow indexes (1 against 0.642), or (ii) the glycerine at 50% and the aqueous solutions of xanthan gum at 1 g/L which have almost the same dimensionless apparent viscosity (589 against 538), but different flow indexes (1 against 0.543). The impact of n_{ost} seems however less pronounced than the one of μ^*.

Fig. 7 compares the dimensionless overall volumetric mass transfer coefficients measured in presence of non-Newtonian fluids with the ones predicted using the process relationship established for Newtonian fluids (Eq. (52)). The points related to each non-Newtonian fluid are regrouped along individual straight lines which are parallel to each others and to the curves previously obtained for Newtonian fluids. This illustrates that the introduction of n_{ost} into the dimensionless modelling (Eq. (54)) could be a mean for differentiating the non-Newtonian fluids from each others and from the Newtonian ones. Nevertheless, this group of four straight lines (one for each fluid) is not classified according to the values of flow index, in particular the associated n_{ost} are not decreasing when deviating from the Newtonian curve (n_{ost} = 1). Indeed, the straight line the closest from the Newtonian curve corresponds to n_{ost} = 0.543 (XG 1 g/L), followed by n_{ost} = 0.373 (XG 2 g/L), then n_{ost} = 0.642 (CMC 4 g/L), until reaching the most distant line, n_{ost} = 0.527 (CMC 6 g/L). This finding tends to show that gathering all the data related to non-Newtonian fluids over the Newtonian ones will be difficult by adding only the flow index n_{ost} in the relevant list. In others words, this would mean that the material function associated with the model of Ostwald–de-Waele could be insufficient and/or unsuitable for describing completely the effect of the shear-thinning properties on $(k_l a)^*$.

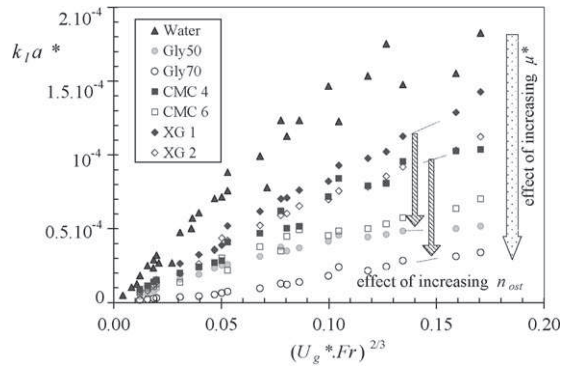

Fig. 6. Effect of dimensionless apparent viscosity and flow index when the Ostwald–de-Waele's model is considered: $(k_l a)^*$ versus $(U_g^* \cdot Fr)^{2/3}$.

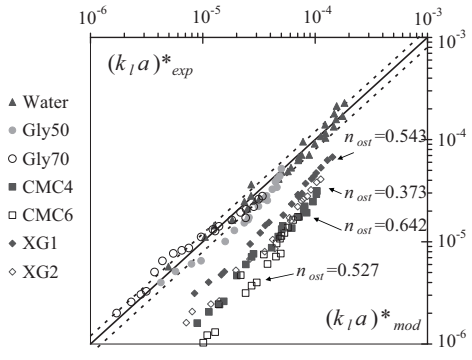

Fig. 7. Modelling using the Ostwald–de-Waele's model: comparison between the experimental $(k_l a)^*$ and the values predicted by Eq. (52) for Newtonian fluids. The dotted lines correspond to a deviation of ±20%.

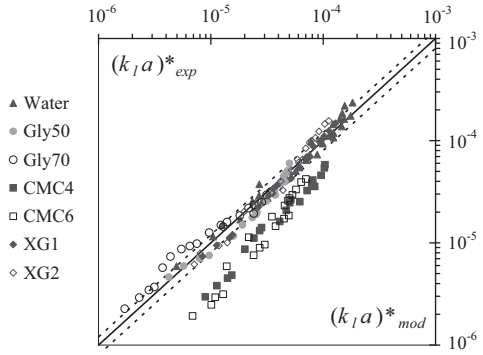

Fig. 8. Modelling using the Ostwald–de-Waele's model: comparison between the experimental $(k_l a)^*$ and the values predicted by Eq. (55). The dotted lines correspond to a deviation of ±20%.

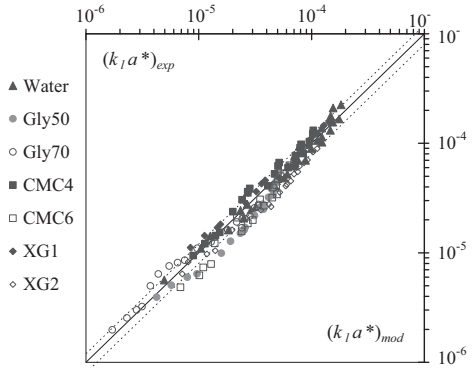

Fig. 9. Modelling using the Williamson's model: comparison between the experimental $(k_l a)^*$ and the values predicted by Eq. (57). The dotted lines correspond to a deviation of ±20%.

The fitting between Eq. (54) and experimental data (determination of the constant α' and the exponent of n_{ost}, the other exponents being the ones of the Newtonian case) leads to:

$$k_l a^* = 0.2284 \cdot (Fr \cdot U_g^*)^{2/3} \cdot (\mu^*)^{-0.591} \cdot (\sigma^*)^{-0.245} \cdot {n_{ost}}^{-1.341}$$
$$\text{valid for} \begin{cases} 0.096 < Fr < 2.4, \quad 0.0029 < U_g^* < 0.029, \quad 54 < \mu^* < 5309 \\ 847 < \rho^* < 1015, \quad 50704 < \sigma^* < 77719, \quad Sc = 7850, \quad 0.37 < n_{ost} < 1 \end{cases} \tag{55}$$

The associated mean standard deviation is equal to 25%. In Fig. 8, the experimental dimensionless mass transfer coefficients $(k_l a)^*$ are reported as a function of the ones predicted by Eq. (55). The exponent of n_{ost} is found negative, and is then coherent with Fig. 6 where the decrease of $(k_l a)^*$ with increasing n_{ost} has been clearly observed. More important, this figure confirms what already suggested in Fig. 7: adding n_{ost} as the single dimensionless ratio in the relevant list (when compared to the Newtonian case) does not enable to gather all the data over the Newtonian curve; in particular, the points related to aqueous solutions of CMC strongly deviate from the others. Thus, the set of dimensionless ratios involved with the Ostwald–de-Waele's model is not able to describe all the complexity of the rheological behaviours encountered in the present aeration experiments (namely the dependency of viscosity with shear rate for the range of fluids under test).

For securing the latter process relationship (Eq. (55)) in a mathematical point of view, two additional cases are tested when implementing the multi-parameter optimization: the first one (Case No. 5) in which σ^* is not taken into account, and the second one (Case No. 6) in which σ^* is taken into account with a non-imposed exponent. The results are collected in Table 8 (Case No. 4 corresponds to Eq. (55)). Whatever the cases, the exponent of n_{ost}, e, remains almost constant, about −1.34 (deviation below 2.6%), and validates thus the robustness of the modelling. The occurrence of a exponent of σ^* (d') has no major effect on the mean standard deviations obtained (25.6% against 25.0%), showing thus that this parameter is neither the one controlling the process relationship nor the additional one enabling to gather all the data.

To conclude, these findings have clearly demonstrated that the use of the Ostwald–de-Waele model is not relevant for encompassing all $(k_l a)^*$ values by a unique process relationship. It is then necessary to visit again the way of characterizing the rheological behaviours, namely the choice of the material function.

Table 8
Dimensionless modelling for non-Newtonian fluids when the Ostwald–de-Waele's model is considered (Eq. (54)).

Case	α'	d'	e	ε (%)
No. 4	**0.2284**	**−0.245**	**−1.341**	***25.2***
No. 5	0.01505	0	−1.377	*25.6*
No. 6	0.04964	−0.107	−1.306	*25.0*

4.3.2. When considering the model of Williamson–Cross

As explained in Section 3.2.2, the reference shear rate, $\dot{\gamma}_o$, is here chosen equal to $1/t_w$ where t_w is a time parameter describing the pseudo-Newtonian behaviour for the smallest shear rates (Eq. (15)). Using such $\dot{\gamma}_o$ and the parameters found when applying the Williamson–Cross's model to experimental rheograms (Fig. 2) leads to the dimensionless numbers collected in Table 7 (sixth, seventh and eighth columns). It can be observed that: (i) the flow index, n_w, have the same order of magnitude than the ones found for the model of Ostwald–de-Waele n_{ost}, (ii) the dimensionless time characteristic number, t_w^*, is a differentiating parameter between the non-Newtonian fluids as being significantly smaller for aqueous solutions of xanthan gum than for the ones of CMC, and (iii) the dimensionless viscosity, μ^*, are now ranged between 108 and 1.59×10^6.

As for Newtonian fluids, the simplest monomial form is looked for the h-function in Eq. (46), and the possible changes in ρ^* and in Sc are neglected. This leads to:

$$k_l a^* = \alpha'' \cdot (Fr)^a \cdot (U_g^*)^b \cdot (\mu^*)^c \cdot (\sigma^*)^d \cdot (n_w)^{e''} \cdot (t_w^*)^f \tag{56}$$

where the exponents of Fr, U_g^*, μ^* and σ^* are the ones determined for the Newtonian case, namely $a = b = 2/3$, $c = -0.591$ and $d = -0.245$. The coefficient α'', the exponents of n_w and of t_w^* (e' and f respectively) are determined by the multi-parameter optimization. The following process relationship is then obtained:

$$k_l a^* = 0.02109 \cdot (Fr \cdot U_g^*)^{2/3} \cdot (\mu^*)^{-0.591} \cdot (\sigma^*)^{-0.245} \cdot (n_w)^{-2.399} \cdot (t_w^*)^{-0.168}$$
$$\text{valid for} \begin{cases} 0.096 < Fr < 2.4, \quad 0.0029 < U_g^* < 0.029, \quad 108 < \mu^* < 1.6.10^6 \\ 847 < \rho^* < 1015, \quad 50704 < \sigma^* < 77719, \\ Sc = 7850, \quad 0.28 < n_w < 1, \quad 3.8.10^{-5} < t_w^* < 1 \end{cases} \tag{57}$$

The associated mean standard deviation is equal to 17.5%, and is thus smaller than the one found when applying the model of Ostwald–de-Waele (Eq. (55)). Fig. 9 plots the experimental dimensionless mass transfer coefficients $(k_l a)^*$ as a function of the ones predicted by Eq. (57). All the points are remarkably grouped together around the data of Newtonian fluids, demonstrating thus the use of the Williamson–Cross's model is relevant for predicting the effect of the non-Newtonian fluids under test on the aeration performances. Then, when the π_i-space is enlarged by two dimensionless ratios to describe the material function (namely n_w and t_w^*), all the aeration experiments can be gathered on a unique curve. This clearly shows that that it is possible to obtain a suitable dimensionless correlation for describing the variations of $k_l a$ at various operating conditions (N, Q_g) and types of fluids, if and only if all the

Table 9
Dimensionless modelling for non-Newtonian fluids when the Williamson–Cross's model is considered (in bold the case retained).

Case	α''	d	e'	f'	ε (%)
No. 7	**0.02109**	**−0.245**	**−2.399**	**−0.1682**	***17.5***
No. 8	0.02090	0	−2.358	−0.1792	*17.5*
No. 9	0.3058	−0.2440	−2.470	−0.1732	*17.4*

rheological properties are correctly taken into account (e.g. using the three parameters involved in the model of Williamson–Cross) instead of neglecting some of them (namely, by simple fitting with the model of Ostwald–de-Waele).

Here also, the mathematical robustness of Eq. (57) is tested by considering several cases when implementing the multi-parameter optimization: in the first case (Case No. 8), the effect of σ^* is neglected whereas, in the second case (Case No. 9), the effect of σ^* is taken into account with a non-imposed exponent. The results are collected in Table 9 (Case No. 7 corresponds to Eq. (57)). They reveal that the occurrence of an exponent of σ^* (d) has a major effect neither on the mean standard deviations nor on the exponents of n_w (e') and of t_w^* (f') which remain almost constant whatever the cases (deviations below 2.4% and 3.2% respectively). Note also that, when the exponent of σ^* is kept free in the optimization, the value found (d) is close to the one already obtained for the Newtonian case. These tests clearly validate Eq. (57) in a mathematical point of view.

In addition, it can be observed that the exponent of t_w^*, and thus the impact of t_w^* on k_la^*, is negative. This is illustrated in Fig. 10 where k_la^* is plotted $(U_g^* \cdot Fr)^{2/3} \cdot \mu^{*-0.591} \cdot {n_w}^{-2.399} \cdot \sigma^{*-0.245}$ (according to the exponents found in Eq. (57) or Case No. 7 in Table 9). The points related to each non-Newtonian fluid are regrouped along individual straight lines which deviate more or less from the curves previously obtained for Newtonian fluids. These straight lines are remarkably classified according to decreasing t_w^* as far as going far from the Newtonian points ($t_w^* = 1$). Thus, at given dimensionless apparent viscosity and flow index, the smallest is the time parameter of the Williamson–Cross's model (t_w) the highest is the overall volumetric mass transfer coefficient (k_la).

All the findings demonstrate that the rigorous extension of the theory of similarity to the case of variable material properties (e.g., dependence of viscosity with shear rate) and the choice of an appropriate material function (here issued from the Williamson–Cross's model) have made possible an accurate dimensionless modelling of the impact of the shear-thinning character of fluids on the aeration performances in a stirred tank. Such approach also enables to understand how each parameter, either operating parameter

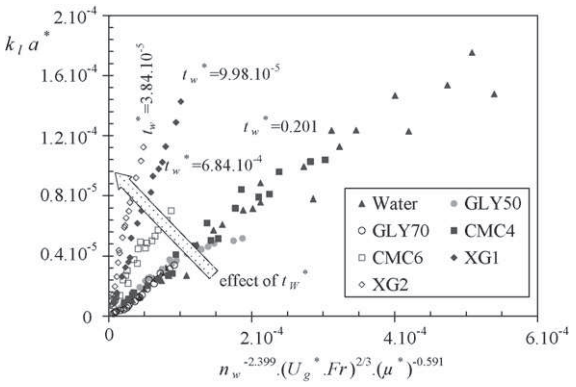

Fig. 10. Effect of dimensionless time parameter of the Williamson's model: $(k_la)^*$ versus $(U_g^* \cdot Fr)^{2/3} \cdot (\mu^*)^{-0.591} \cdot (n_w)^{-2.399} \cdot (\sigma^*)^{-0.245}$.

(such as rotational impeller speed or gas flow rate) or material parameter (such as surface tension, apparent viscosity, flow index or Williamson–Cross time parameter), acts individually on the overall volumetric mass transfer coefficient. The correlation established (Eq. (57)) is at present validated in the range of dimensionless numbers previously defined, for a given temperature, under a given pressure and for the agitation/aeration system used (in particular for $H_l/T_t = 1$, $D/T_t = 0.4$, $D_s/T_t = 0.75$ and for the other geometrical ratios characteristics of the present system). Further experiments are now required to:

- to evaluate the effect of the Schmidt number on k_la^*; for that, the diffusion coefficient of oxygen in the viscous fluids under test have to be experimentally measured.
- to definitively appreciate the validity of such process relationship when extending out of the domain investigated in the present study (for example at larger tank, at higher gas hold-up and for different types of agitation systems).

5. Conclusion

The present paper dealt with a consistent dimensionless analysis of gas–liquid mass transfer in an aerated stirred tank containing purely viscous fluids with shear-thinning fluids. More particularly, this work showed how to proceed:

- to construct a complete list of relevant parameters able to build an unique π-space which keeps unchanged for both Newtonian and non-Newtonian fluids.
- and consequently to elaborate, without pitfalls, a set of dimensionless numbers characterizing all the factors governing absorption rate coefficients (k_la) in a stirred tank where shear-thinning fluids are involved.

This theoretical approach was supported by a set of k_la measurements in a tank stirred by a six-concave-blade disk turbine and aerated by a ring sparger, under different operating conditions (rotational impeller speed, gas flow rate) and for various fluids (water, glycerine 50% and 70%, solutions of CMC at 4 and 6 g/L, solutions of xanthan gum at 1 and 2 g/L). These measures were validated notably by means of two methods (physical and chemical). At last, a suitable dimensionless correlation could be obtained for describing all the variations of k_la if and only if all the rheological properties were correctly taken into account (e.g. using the three parameters involved in the model of Williamson–Cross) instead of neglecting some of them (namely, by simple fitting with the model of Ostwald–de-Waele. It was expressed by:

$$k_la^* = 0.02109 \cdot (Fr \cdot U_g^*)^{2/3} \cdot (\mu^*)^{-0.591} \cdot (\sigma^*)^{-0.245} \cdot (n_w)^{-2.399} \cdot (t_w^*)^{-0.168}$$

$$\text{valid for} \begin{cases} 0.096 < Fr < 2.4, \quad 0.0029 < U_g^* < 0.029, \quad 108 < \mu^* < 1.6.10^6 \\ 847 < \rho^* < 1015, \quad 50704 < \sigma^* < 77719, \\ Sc = 7850, \quad 0.28 < n_w < 1, \quad 3.8.10^{-5} < t_w^* < 1 \end{cases}$$

In the future, further experiments will be required to definitively appreciate the effect of Schmidt number and the validity of such process relationship when extending out of the domain investigated in the present study (for example at larger tank).

This paper constitutes then an eloquent example demonstrating how the variability of physical material parameters in a process equipment should be integrated. The advantage of such approach is to be perfectly transposable to any other physical properties and other unit operation involving material with non-constant properties.

References

[1] J.B. Joshi, A.B. Pandit, M.M. Sharma, Mechanically agitated gas–liquid reactors, Chem. Eng. Sci. 37 (6) (1982) 813–844.
[2] E.L. Paul, V.A. Atiemo-Obeng, S.M. Kresta, Handbook of Industrial Mixing: Science and Practise, J. Wiley & sons, 2004.
[3] F. Garcia-Ochoa, E. Gomez, Bioreactor scale-up and oxygen transfer rate in microbial processes: an overview, Biotechnol. Adv. 27 (2009) 153–176.
[4] M. Martin, F.J. Montes, M.A. Galan, Bubbling process in stirred tank reactors. II. Agitator effect on the mass transfer rates, Chem. Eng. Sci. 63 (2008) 3223–3234.
[5] M. Martin, F.J. Montes, M.A. Galan, Mass transfer rates from bubbles in stirred tanks operating with viscous fluids, Chem. Eng. Sci. 65 (2010) 3814–3824.
[6] K. Van't Riet, Review of measuring methods and results in non-viscous gas–liquid mass transfer in stirred vessels, Ind. Eng. Chem. Process Des. Dev. 18 (3) (1979) 357–364.
[7] M. Zlokarnik, Sorption characteristics for gas–liquid contacting in mixing vessels, Adv. Biochem. Eng. 8 (1979) 133–157.
[8] H. Judat, Gas/liquid mass transfer in stirred vessels - a critical review, Ger. Chem. Eng. 5 (1982) 357–363.
[9] V. Schlüter, W.D. Deckwer, Gas–liquid mass transfer in stirred vessels, Chem. Eng. Sci. 47 (9–11) (1992) 2357–2362.
[10] M. Roustan, A. Liné, Rôle du brassage dans les procédés biologiques d'épuration, Tribune de l'Eau 49 (1996) 109–115.
[11] J.F. Perez, O.C. Sandall, Gas absorption by non-Newtonian fluids in agitated vessels, AIChE J. 20 (1974) 770.
[12] H. Yagi, F. Yoshida, Gas absorption by Newtonian and non-Newtonian fluids in sparged agitated vessel, Ind. Eng. Chem. Process Des. Dev. 14 (1975) 488–493.
[13] M. Nishikawa, M. Nakamura, H. Yagi, K. Hashimoto, Gas absorption in aerated mixing vessels, J. Chem. Eng. Jpn. 14 (3) (1981) 219–226.
[14] M. Nishikawa, M. Nakamura, K. Hashimoto, Gas absorption in aerated mixing vessels with non-Newtonian liquid, J. Chem. Eng. Jpn. 14 (3) (1981) 227–232.
[15] E. Costa, A. Lucas, J. Aguado, J.A. Avila, Transferencia de materia en tanques agitados: burbujeo de gases en líquidos newtonianos y no newtonianos. I. Turbinas de 6 paletas y difusor plano, An. Quim. 78 (1982) 387–392.
[16] R.S. Albal, Y.T. Shah, A. Schumpe, N.L. Carr, Mass transfer in multiphase agitated contactors, Chem. Eng. J. 27 (1983) 61–80.
[17] F. Garcia-Ochoa, E. Gomez, Mass transfer coefficient in stirred tank reactors for xanthan gum solution, Biochem. Eng. J. 1 (1998) 1–10.
[18] C. Xuereb, M. Poux, J. Bertrand, Agitation et mélange: Aspects fondamentaux et applications industrielles, L'Usine Nouvelle Dunod, 2006.
[19] R. Hassan, J. Loubière, J. Legrand, Gas–liquid mass transfer in a stirred tank for non-Newtonian fluids. Application to the autothermal thermophilic digestion of sludge, in: 9th International Congress of Chemical and Process Engineering (CHISA), Prague, Czech Republic, 2010.
[20] W.K. Lewis, W.G. Whitman, Principles of gas absorption, Ind. Eng. Chem. 16 (1974) 1215–1220.
[21] J. Ingham, I.J. Dunn, E. Heinzle, J.E. Prenosil, Chemical Engineering Dynamics. Modeling with PC Simulation, VCH Publishers Inc., New York, 1994, ISBN 3-527-28577-6.
[22] C.O. Vandu, K. Koop, R. Krishna, Volumetric mass transfer coefficient in a slurry bubble column operating in the heterogeneous flow regime, Chem. Eng. Sci. 59 (2004) 5417–5423.
[23] J.K. Bewtra, W.R. Nicholas, L.B. Polkowski, Effect of temperature on oxygen transfer in water, Water Res. 4 (2) (1970) 115.
[24] F. F. Cabaret, L. Fradette, P.A. Tanguy, Gas–liquid mass transfer in unbaffled dual-impeller mixers, Chem. Eng. Sci. 63 (2008) 1636–1647.
[25] V. Linek, V. Vacek, P. Benes, A critical review and experimental verification of the correct use of the dynamic method for the determination of oxygen transfer in aerated agitated vessels to water, electrolyte solutions and viscous liquids, Chem. Eng. J. 34 (1987) 11–34.
[26] A.S. Khare, K. Niranjan, Impeller-agitated aerobic reactor: the influence of tiny bubbles on gas hold-up and mass transfer in highly viscous liquids, Chem. Eng. Sci. 50 (7) (1995) 1091–1105.
[27] P. Painmanakul, K. Loubière, G. Hébrard, M. Mietton-Peuchot, M. Roustan, Effect of surfactants on liquid-side mass transfer coefficients, Chem. Eng. Sci. 60 (2005) 6480–6491.
[28] L.-K. Ju, C.S. Ho, The structure-breaking effect on oxygen diffusion coefficients in electrolyte and polyelectrolyte solutions, Can. J. Chem. Eng. 67 (1989) 471–476.
[29] T. Espinosa-Solares, E. Brito-De La Fuente, A. Tecante, P.A. Tanguy, Gas dispersion in rheologically-evolving model fluids by hybrid dual mixing systems, Chem. Eng. Technol. 25 (7) (2002) 723–727.
[30] M. Hilal, Etude de l'écoulement d'un fluide non Newtonien à travers les réacteurs à lit fixe: chute de pression, dispersion axiale et transfert de matière, Thèse de doctorat, Université of Nantes N 91 NANT 2049, 1991.
[31] M. Mori, J. Isaac, I. Seyssiecq, N. Roche, Effect of measuring geometries and of exocellular polymeric substances on the rheological behaviour of sewage sludge, Chem. Eng. Res. Des. 86 (2008) 554–559.
[32] M. Zlokarnik, Scale-up in Chemical Engineering Second, Completely Revised and Extended edition, Wiley-VCH Verlag GmbH & Co., 2006.
[33] T. Szirtes, Applied Dimensional Analysis and Modelling, McGraw-Hill, New York, 1998.
[34] J. Pawlowski, Die ähnlichkeitstheorie in des physikalissch-technischen Forschung- Grundlagen und Anwendungen, Springer Verlag, Berlin/Heidelberg/New York, 1971.
[35] E.N. Seider, G.E. Tate, Heat transfer and pressure drop of liquids in tubes, Ind. Eng. Chem. 28 (1936) 1429.
[36] M. Zlokarnik, Scale-up of processes using material systems with variable physical properties, Chem. Biochem. Eng. Q 15 (2) (2001) 43–47.
[37] R. Hassan, Etude expérimentale et modélisation du transfert de matière gaz-liquide en cuve agitée en présence de fluides non-Newtoniens simulant des boues de station d'épuration, Thesis, University of Nantes, 2011.